Highly-translucent, strong and aging-resistant 3Y-TZP ceramics for dental restoration by grain boundary segregation

Reference:

Zhang Fei, Vanmeensel Kim, Batuk Maria, Hadermann Joke, Inokoshi Masanao, Van Meerbeek Bart, Naert Ignace, Vleugels Jef.- Highly-translucent, strong and aging-resistant 3Y-TZP ceramics for dental restoration by grain boundary segregation
Acta biomaterialia - ISSN 1742-7061 - 16(2015), p. 215-222
DOI: http://dx.doi.org/doi:10.1016/j.actbio.2015.01.037
Handle: http://hdl.handle.net/10067/1244210151162165141

Highly-translucent, Strong and Aging-resistant 3Y-TZP ceramics for Dental Restoration by Grain Boundary Segregation

Fei Zhang[a*], Kim Vanmeensel[a], Maria Batuk[b], Joke Hadermann[b], Masanao Inokoshi[c], Bart Van Meerbeek[c], Ignace Naert[c], Jef Vleugels[a]

[a] Department of Materials Engineering, KU Leuven, Kasteelpark Arenberg, 44, B-3001 Heverlee, Belgium

[b] Electron Microscopy for Materials Science (EMAT), University of Antwerp, Groenenborgerlaan 171, B-2020 Antwerp, Belgium

[c] KU Leuven BIOMAT, Department of Oral Health Sciences, KU Leuven & Dentistry, University Hospitals Leuven, Kapucijnenvoer, 7, blok a, B-3000 Leuven, Belgium

*Corresponding author. Tel.: +32 16 37 77 38.

E-mail address: fei.zhang@mtm.kuleuven.be (F. Zhang)

Abstract

Latest trends in dental restorative ceramics involve the development of full-contour 3Y-TZP ceramics which can avoid chipping of veneering porcelains. Amongst the challenges are the low translucency and the hydrothermal stability of 3Y-TZP ceramics. In this work, different trivalent oxides (Al_2O_3, Sc_2O_3, Nd_2O_3 and La_2O_3) were selected to dope 3Y-TZP ceramics. Results show that dopant segregation was a key factor to design hydrothermally stable and high-translucent 3Y-TZP ceramics and the cation dopant radius could be used as a controlling parameter. A large trivalent dopant, oversized as compared to Zr^{4+}, exhibiting strong segregation at the ZrO_2 grain boundary was preferred. The introduction of 0.2 mol% La_2O_3 in conventional 0.1-0.25 wt.% Al_2O_3-doped 3Y-TZP resulted in an excellent combination of high translucency and superior hydrothermal stability, while retaining the excellent mechanical properties.

Keyword: Ceramic structure; Dental restorative material; Zirconia; Aging; Translucency

1. Introduction

The increased aesthetic demands of patients for both anterior and posterior teeth are driving the development of dental restorative materials from traditional porcelain-fused-to-metal (PFM) to all-ceramic restorations [1, 2]. Yttria-stabilized tetragonal zirconia polycrystalline (Y-TZP) ceramics, commonly containing 3 mol% yttria, have been widely accepted as a promising material for fabricating dental crowns and fixed dental prostheses (FDP) because of their superior biocompatibility [3], excellent mechanical properties and high aesthetic potential [4-6]. The brittleness of most dental restorative ceramics limited their use only for small anterior restorations [1]. 3Y-TZP ceramics are tough and strong, allowing the fabrication of larger all-ceramic restorations and in the highly-loaded molar area [4, 7, 8], which is mainly due to the transformation toughening effect of submicrometer sized tetragonal zirconia [9, 10].

However, 3Y-TZP ceramics suffer from low-temperature degradation (LTD), i.e. the spontaneous transformation of the tetragonal to monoclinic ZrO_2 phase in the presence of water (hydrothermal aging) [11, 12]. Hydrothermal aging can result in enhanced wear rates with the release of small zirconia particles in the surrounding environment, roughening of the surface finish, aesthetic degradation, loss of mechanical properties and even catastrophic failure [12-14]. Long-term stability of Y-TZP ceramics is therefore crucial for biomaterial applications.

Adding a small amount of alumina has proven to be effective in increasing the aging resistance of 3Y-TZP ceramics [15]. 0.25 wt.% alumina was normally added, but lower amounts of alumina (to 0.1 or 0.05 wt.%) are used in the new generations of high-translucent 3Y-TZP ceramics [5, 16].

The low translucency of conventional 3Y-TZP ceramics is its major drawback to mimic the optical properties of natural tooth enamel [17, 18]. An esthetic porcelain veneer is therefore needed to cover the opaque zirconia. However, chipping or de-bonding of the veneering porcelain from the zirconia

framework is commonly reported in clinics [14, 19]. Although fracture of the strong zirconia substructure is rarely reported, the contribution of strong core materials to the performance of all-ceramics restorations was obviously offset by the veneering fractures [20]. Therefore, high-translucent Y-TZP ceramics are becoming popular in restorative dentistry in order to make full-contour zirconia restorations without the need for aesthetic veneering porcelain [21-23].

Although lowering the amount of alumina addition from 0.25 to 0.1 or 0.05 wt% can increase the translucency, the hydrothermal stability is simultaneously lowered [16, 24]. Moreover, hydrothermal aging of full-contour Y-TZP restorations could be more crucial, since they are in direct contact with the oral fluid. On the other hand, another strategy of increasing the yttria content and introducing cubic phase zirconia was also used to improve the translucency of Y-TZP ceramics [5, 16, 25]. Aging-resistant Y-TZP ceramics can be obtained, but this strategy sacrifices their excellent flexural strength and fracture toughness due to the partial loss of the transformation toughening effect of tetragonal zirconia [5, 26].

Therefore, the aim of this work was to design hydrothermally stable and high-translucent 3Y-TZP ceramics while retaining their inherent excellent mechanical properties.

The macroscopic properties of polycrystalline materials depend on the grain size and the atomic structure and chemistry of the grain boundaries. As a birefringent material, the optical properties of Y-TZPs are strongly influenced by the structure of the grain boundaries [27]. The chemistry of the zirconia grain boundary was reported to be critical for the aging behavior of Y-TZP ceramics [28-30]. Furthermore, the phase composition [31] and grain size [32] of Y-TZP ceramics are controlled by the grain boundary structure, which in turn influences the translucency [5, 33], aging behavior [13] and mechanical properties [34]. Therefore, in this work, we explored the strategy of controlling the

composition of the zirconia grain boundaries at the nanometer level using the atomic radius of an additional dopant oxide as a grain boundary engineering tool.

2. Materials and methods

2.1. Material preparation

Pure tetragonal zirconia was doped with trivalent oxides having a different cation radius Al^{3+} (53.5 pm) < Zr^{4+} (84.0 pm) ~ Sc^{3+} (87.0 pm) < Y^{3+} (101.9 pm) < Nd^{3+} (110.9 pm) < La^{3+} (116.0 pm) [35]. Formulations were made with each of the trivalent oxides (Nd_2O_3 (Chempur, purity of 99.9%), La_2O_3 (Chempur, purity of 99.99%), Sc_2O_3 (abcr GmbH & Co. KG, purity of 99.9%), Al_2O_3 (TM-DAR, purity of 99.99%)) by mixing with tetragonal ZrO_2 nanopowder (grade TZ-3Y, Tosoh, Japan) on a multidirectional mixer (Turbula type T2C, Basel, Switzerland) for 24 h in ethanol using 5 mm Y-TZP milling balls. The mol% was indicated in the nomenclature expect for the Al_2O_3 dopant which was indicated in wt.% (for example 3Y-0.1La means 3 mol% Y_2O_3 and 0.1 mol% La_2O_3, 3Y-0.25Al means 3 mol% Y_2O_3 and 0.25 wt.% Al_2O_3).

The mixed suspension was further processed by bead milling (DISPERMAT®SL, Germany) for 3 h at 5000 rpm using 1 mm ZrO_2 beads (grade TZ-3Y, Tosoh, Japan). A reference tetragonal zirconia powder with 0.25 wt.% alumina (grade TZ-3Y-E, Tosoh, Japan) was mixed and bead milled for comparison. Alumina-free 3Y-TZP was made from Tosoh TZ-3Y (grade TZ-3Y, Tosoh, Japan) as a reference material for the translucency measurement. All powders were cold isostatically pressed at 250 MPa for 1 minute and pressureless sintered in air at 1450 ℃ or 1500 ℃ for 2 h. The density of the sintered ceramics was measured according to the Archimedes principle in ethanol.

2.2. Microstructural characterizations

Scanning electron microscopy (SEM, XL-30FEG, FEI, Eindhoven, The Netherlands) was used to characterize the microstructure on polished thermally etched (1250 ℃ for 25 min in air) and Pt-coated

surfaces. The grain size was measured on SEM micrographs using IMAGE-PRO software according to the linear intercept method. At least 1000 grains were counted, and the average results (± standard deviation) were reported without any correction. ANOVA and unpaired two sample *t*-tests were performed using statistical analysis software (Minitab® 16.2.1, Pennsylvania, USA) to identify significant differences in the mean values between different samples.

Transmission electron microscopy (TEM) analysis was performed to examine the distribution of dopant cations (La^{3+}, Nd^{3+}, Al^{3+} or Sc^{3+}), $Y^{3+}$and Zr^{4+} around the grain boundaries. Electron transparent samples were prepared by ion-milling with an Ion Slicer (EM-09100IS, Jeol, Japan). High angle annular dark field scanning transmission electron microscopy (HAADF-STEM) images and energy-dispersive spectroscopy (STEM-EDS) elemental maps were obtained on a FEI Titan 60-300 "cubed" transmission electron microscope operated at 200 kV. 5-7 grain boundaries in each ceramic were analysed. Quantitative elemental mappings were acquired to calculate the element concentration profile across the grain boundary using ESPRIT 1.9 software.

2.3. Assessment of aging kinetics

In vitro accelerated hydrothermal experiments were used to age the ceramics. Double-side mirror polished specimens were autoclaved at 134 ℃ and 0.2 MPa in water vapour. The amount of tetragonal to monoclinic phase transformation was determined by X-ray diffraction (XRD, 3003-TT, Seifert, Ahrensburg, Germany) using Cu-K_α radiation at 40 kV and 40 mA. XRD patterns were recorded in the range of 27-33 ° (2θ) by θ-2θ mode with a scan speed of 2 s/step and a scan size of 0.02 ° (the X-ray penetration depth was calculated to be 7.5 μm (Cu-K_α with 98% absorption)). The monoclinic phase content (V_m) was calculated according to the formula of Garvie et al. [36] and Toraya et al. [37].

$$V_m = \frac{1.311 * (I_m^{-111} + I_m^{111})}{1.311 * (I_m^{-111} + I_m^{111}) + I_t^{101}} \quad (1)$$

With *I*, the intensity of monoclinic (-111 and 111) and tetragonal (101) phase peaks indicated by the subscripts *m* and *t*.

The monoclinic phase content was plotted as a function of aging time to indicate the aging kinetics. For each curve, at least 3 specimens (6 exposed surfaces) were tested and the average result was reported. Note that, at 0 h of aging, XRD patterns were recorded in the range of 20-90 °(2θ) to identify the phase composition of non-aged specimen.

Furthermore, in order to compare the aging kinetics of different ceramics, the aging kinetics were rationalized by fitting the transformation curves with the Mehl–Avrami–Johnson (JMA) equation, as follows [11]:

$$\frac{V_m}{V_{ms}} = 1 - \exp(-(bt)^n) \quad (2)$$

where V_m is the monoclinic phase content, V_{ms} the monoclinic zirconia content saturation level, b (h^{-1}) the parameter describing the effective kinetics of the tetragonal to monoclinic phase transformation during the aging process [11, 38], and n the parameter related to the geometry of the transformation [39].

Moreover, the transformation propagation was investigated on polished cross-sections by SEM.

2.4. Characterization of mechanical properties

The hardness and fracture toughness were measured by the indentation method using a Vickers microhardness tester (Model FV-700, Future-Tech Corp., Tokyo, Japan) with a load of 98 N, and the indentation toughness of all ceramics was calculated according to the Anstis equation [40] with an E-modulus value of 210 GPa. Ten indentations were applied for each ceramic grade.

The four-point bending strength was measured on 45×4×3 mm^3 test bars (10 bars for each material). Bending bars were prepared according to ISO 13356 [41] and ISO 6872 [42] but without 45° edge chamfer.

2.5. Translucency measurement

Six disk-shaped 15 mm diameter 3Y-TZP specimens of each composition were prepared for translucency measurements. The discs were ground plan parallel to a thickness of 0.5 mm and polished with wet 3 µm-grit diamond lapping film. The final thickness was controlled during the polishing process with a digital micrometre (accuracy of 0.001 mm). After polishing, the surface roughness was measured with a surface profiler (Talysurf-120L, Taylor Hobson) to ensure an identical roughness level for all ceramic grades.

A dental spectrophotometer (SpectroShade^{TM} MICRO, MHT Optic Research, Niederhasli, Switzerland) with a calibration plate was used to record the CIELAB coordinates (L*, a* and b*) of the ceramic discs. A layer of vaseline was put in-between the specimen and the background for better optical contact.

The translucency parameter (TP) was determined by calculating the colour difference between the same specimen against black and white backgrounds, according to the following equation [43]**:**

$$\mathrm{TP} = \sqrt{(L_B^* - L_W^*)^2 + (a_B^* - a_W^*)^2 + (b_B^* - b_W^*)^2} \quad (2)$$

where the subscripts B and W refer to the colour coordinates over black and white backgrounds, respectively. A higher TP value indicates a higher translucency.

The contrast ratio (CR) is also commonly used to indicate the translucency of ceramics in the dental community. The CR is defined as the ratio of illuminance (Y) of the test material placed on a black (Y_b)

and a white (Y_w) background. The value of Y was calculated with the L* value measured with the spectrophotometer, as follows [43]:

$$Y = (\frac{L^* + 16}{116})^3 \times Y_n \quad (3)$$

For simulated object colours, the specified white stimulus normally chosen is one that has the appearance of a perfect reflecting diffuser, normalized by a common factor so that Y_n is equal to 100 [44]. CR is 0.0 for a transparent material and 1.0 for a totally opaque material. The CR value linearly correlates with the TP value [43].

3. Results and discussion

3.1. Influence of the cation radius on the aging kinetics of 3Y-TZP

Trivalent oxides (Al_2O_3, Sc_2O_3, Nd_2O_3 and La_2O_3) were selected to dope 3Y-TZP ceramics with a different cation radius Al^{3+} (53.5 pm) < Zr^{4+} (84.0 pm) ~ Sc^{3+} (87.0 pm) < Y^{3+} (101.9 pm) < Nd^{3+} (110.9 pm) <La^{3+} (116.0 pm) [35]. Note that only a small amount of dopant was added to the 3Y-TZP ceramic to retain the tetragonal zirconia phase for the benefit of active transformation toughening.

Fig. 1a shows the monoclinic phase content as a function of aging time on a logarithmic time scale, revealing that the hydrothermal stability of 3Y-TZP ceramics is strongly influenced by the cation type. Sc_2O_3-doped 3Y-TZP degraded fastest, although the ionic radius of Sc^{3+} was neither the largest nor the smallest. Characterization of the local chemistry of the zirconia grain boundaries (Fig. 1b) showed that Al^{3+}, Nd^{3+} and La^{3+} segregated to the outer 5 nm of the ZrO_2 grains, whereas Sc^{3+} did not. Therefore, dopant cation segregation to the grain boundaries play a key role in retarding the aging rate of 3Y-TZP ceramics, which strongly supports earlier statements about the favorable effects of different dopants (including Al_2O_3, La_2O_3, MgO and GeO_2) [28, 29, 45]. Divalent and trivalent oxides were reported to be able to segregate to the zirconia grain boundaries in Y-TZP ceramics [32], while it is shown here

that the cation radius was critical as well. A significant driving force for the segregation can be the large size mismatch between the dopant and host cations [46]. Since the mismatch between Sc^{3+} (87.0 pm) and Zr^{4+} (84.0 pm) is small, Sc^{3+} did not segregate at the ZrO_2 grain boundary but homogeneously dispersed throughout the zirconia grains. The absence of segregation in Sc_2O_3-doped zirconia is also consistent with the low solution energy of incorporating Sc_2O_3 into a ZrO_2 lattice [47, 48]. La^{3+} and Nd^{3+} are substantially larger than Zr^{4+} explaining the segregation. The solubility of Al_2O_3 in zirconia is low at room temperature, resulting in the segregation of Al^{3+} during cooling from the sintering temperature [47].

More importantly, Fig.1a shows that the hydrothermal stability increased with increasing dopant cation radii (La^{3+} > Nd^{3+} > Al^{3+}), even though La^{3+}, Nd^{3+} and Al^{3+} all segregated at the zirconia grain boundary (Fig.1b). This difference should originate from a different diffusivity of water species into the lattice via oxygen vacancies and a different zirconia grain size. The filling of oxygen vacancies by "water-derived species" (probably in the form of OH^-) at the grain boundary is believed to trigger the hydrothermal aging of Y-TZP ceramics [30, 49]. The segregated trivalent cations (M'_{Zr}) bind the oxygen vacancies ($V_o^{\cdot\cdot}$) [47, 48] at the grain boundary and strongly interrupt the annihilation of oxygen vacancies. It can therefore be expected that the aging kinetics depend on the binding energy of defect clusters [$M'_{Zr} \cdot V_o^{\cdot\cdot}$] which in turn depend on the dopant cation radius [47, 48]. According to atomistic simulations, the binding energy is minimal for [$Sc'_{Zr} \cdot V_o^{\cdot\cdot}$] and increases as the dopant cation size increases for oversized trivalent dopants (i.e. larger than Sc^{3+}) or as the dopant cation size decreases for undersized trivalent dopants [47, 48]. In order to retard the aging kinetics, larger oversized dopant cations (such as La^{3+}) and smaller undersized dopant cations (such as Al^{3+}) are thus preferred due to the stronger bonding of the oxygen vacancy. Furthermore, larger oversized cations are more preferred because of their grain growth inhibiting effect on tetragonal zirconia [32] and concomitant higher degradation resistance. The grain boundary mobility depends on the diffusivity and the segregation of

impurities at the grain boundary [32]. When La^{3+}, Nd^{3+} and Al^{3+} segregated at the zirconia grain boundary, the grain boundary diffusivity decreased as the dopant radius increased [32]. Therefore, the grain size of the La_2O_3-doped 3Y-TZP was the smallest (213 ± 90 nm), followed by that of Nd_2O_3- (252 ± 111 nm) and Al_2O_3- (305 ± 127 nm) doped 3Y-TZP (Fig .1c, differences between each other are all significant with $P < 0.001$ (ANOVA and *t*-test)). The smaller grain size resulted in a most stable La_2O_3-doped 3Y-TZP. In addition, a smaller grain size was expected to be beneficial for the higher translucency of fully dense TZP ceramics [5, 27], a smaller critical flaw size and concomitantly higher strength [50]. La_2O_3 therefore appeared to be the most potent dopant, motivating to examine the effect of La_2O_3 concentration.

3.2. Optimum amount of La_2O_3 dopant

The addition of 0.2-0.4 mol% La_2O_3 led to the highest ageing resistance of the 3Y-TZP ceramics and the zirconia grain size was smallest at 0.4 mol% La_2O_3 addition (Table 1). The hydrothermal stability of 3Y-TZP increased when the amount of La_2O_3 increased from 0.02 to 0.4 mol% but decreased when the amount of La_2O_3 was further increased (Fig. 2a and see also the value of the ageing kinetic parameter b in Table 1). A secondary $La_2Zr_2O_7$ phase precipitated at La_2O_3 contents ≥ 1 mol% (Fig. 2b). This secondary phase can enhance the aging of Y-TZP ceramics due to the accompanied volume expansion [51], and can also deteriorate the translucency of Y-TZP ceramics as a light scattering source.

Current results described above and a previous study about the amount of alumina addition [52] showed that not only the type of dopant but also the amount of dopant were critical for designing aging-resistant 3Y-TZP ceramics. Only the segregation of trivalent cations at the zirconia grain boundaries was effective to retard the degradation of Y-TZPs, so the optimum amount of dopant addition should be the maximum amount of dopant that can be dissolved at the zirconia grain boundaries after cooling without precipitation of secondary phases.

On the other hand, the challenge for La_2O_3-doped 3Y-TZP is densification. A density of ≥ 6.00 g/cm^3 is required for the application of 3Y-TZP as a load-bearing biomaterial [41]. However, all La_2O_3-doped 3Y-TZP, even with a very low dopant content of 0.02 mol%, were not fully densified after pressureless sintering at 1500 ℃ for 2 h (Table 1). Residual porosity was clearly observed on SEM images of polished cross-sections, resulting in a reduced hardness (Table 1). The residual porosity can also significantly deteriorate the translucency of Y-TZP [5, 33]. Therefore, co-doping of La_2O_3 and Al_2O_3 was a final option, since alumina is a commonly used sintering aid in 3Y-TZP ceramics. 3Y-TZPs with the addition of 0.1-0.4 mol% La_2O_3 and 0.1-0.25 wt% Al_2O_3 could indeed be fully densified when sintered for 2 h at 1450 or 1500 ℃.

3.3. La_2O_3 and Al_2O_3 co-doping in 3Y-TZP

Eventually, 0.2 mol% La_2O_3 and 0.1-0.25 wt% Al_2O_3 co-doped 3Y-TZP showed an excellent combination of long-term hydrothermal stability (Fig. 3a and Fig. 3b), translucency (Fig. 3d and Table 2), and good mechanical properties (Fig. 3e and Table 3), when compared to 3Y-E (0.25Al) processed from the most commonly used zirconia powder grade (Tosoh TZ-3Y-E, E means 0.25 wt% alumina) for dental applications.

The translucency of 3Y-0.2La-0.25Al and 3Y-0.2La-0.1Al was much higher than that of 3Y-E (0.25Al), even though the amount of alumina in 3Y-0.2La-0.25Al was the same as in 3Y-E (0.25Al). The translucency of 3Y-0.2La-0.25Al and 3Y-0.2La-0.1Al was even higher than for alumina-free 3Y-TZP ceramics (Ref. 3Y). The highest translucency parameter, 22.6 for 0.5 mm thick discs, measured for 3Y-0.2La-0.1Al was about 42% higher than for the conventional 3Y-E ceramic. This benefits from the combined effects of high density, the absence of secondary phases, smaller porosity and less birefringence at the grain boundaries in 3Y-0.2La-0.25Al and 3Y-0.2La-0.1Al.

Secondary phase alumina particles were clearly observed in the 3Y-E (0.25Al) ceramic (Fig. 3c), which strongly scattered the incoming light since the refractory index of alumina and zirconia is different [16, 53]. However, when La_2O_3 and Al_2O_3 are co-doped, the 0.2 mol% La_2O_3 dopant completely dissolved in the zirconia grains without secondary phase precipitation. SEM images confirmed that 3Y-0.2La-0.1Al was free of secondary phases, whereas 3Y-0.1La-0.25Al contained a very small amount of alumina grains (Fig. 3c). Moreover, a finer microstructure was obtained by La_2O_3 doping (Fig. 3c, Table 3, $P < 0.001$ (*t*-test with reference 3Y-E)), which should improve the optical transmission due to a smaller porosity [33, 54], a narrow grain boundary width and a high in-line transmission [5, 27, 54]. Although porosity was scarcely observed in all 3Y-TZP ceramics compared in Fig. 3c, it has been reported that even a very small amount of porosity influences the translucency. Furthermore, residual porosity (not only the amount of porosity but also the size of porosity) are even more important than grain boundaries [33]. Last but not least, larger trivalent dopants prefer an 8-fold oxygen coordination, enhancing the adoption of a cubic zirconia symmetry [47, 55]. Since cubic zirconia is optical isotropic, it is possible that the La^{3+}-doped ZrO_2 grain boundary has a reduced birefringence effect.

Significantly, unlike the approach of lowering the alumina content or increasing the yttria content, the strategy of introducing La_2O_3 dopant allowed the combination of superior aging resistance and mechanical property while obtaining a higher translucency. Fig. 3a shows that 3Y-0.2La-0.1Al and 3Y-0.2La-0.25Al degraded slower than 3Y-E when sintered at 1450-1500 ℃ (the optimal sintering temperature for this powder). In particular, 3Y-0.2La-0.1Al and 3Y-0.2La-0.25Al did not show any phase transformation up to 120 h of hydrothermal treatment at 134 ℃ when sintered at 1450 ℃. Although 3Y-0.2La-0.1Al degraded faster than 3Y-0.2La-0.25Al, it degraded slower than 3Y-E (0.25Al) (the depth of transformation in Fig. 3b confirmed this result). Furthermore, the fracture toughness, hardness and flexural strength of 3Y-0.2La-0.1Al and 3Y-0.2La-0.25Al was comparable to

that of 3Y-E (Table 3) because we maintained the sub-micrometer sized grains in all 3Y-TZP ceramics with tetragonal phase crystallography (Fig. 2b). A previous study confirms the finding that co-doping of 3Y-TZP with a small amount of alumina and lanthania can dramatically retard its aging rate without any loss of fracture toughness, and the segregation of Al^{3+} and La^{3+} fundamentally changed the transformation kinetics from nucleation-driven to growth-driven [29]. In the present study, a higher translucency was found to be an additional favorable effect of La_2O_3 addition (optimum 0.2 mol%) for restorative 3Y-TZP ceramics.

4. Conclusion

In summary, dopant segregation was found to be a key factor to design hydrothermally stable and high-translucent 3Y-TZP ceramics and the cation dopant radius could be used as a controlling parameter. A large trivalent dopant, oversized as compared to Zr^{4+}, exhibiting strong segregation at the ZrO_2 grain boundary was preferred. The introduction of 0.2 mol% La_2O_3 in conventional Al_2O_3-doped 3Y-TZP resulted in a unique combination of high translucency (42% increase compared to conventional 0.25 wt.% alumina-doped 3Y-TZP) and superior hydrothermal stability (no transformation up to 120 h of hydrothermal aging at 134 ℃), while maintaining the excellent mechanical properties.

Acknowledgements

We acknowledge the Research Fund of KU Leuven under project 0T/10/052 and the Fund for Scientific Research Flanders (FWO-Vlaanderen) under grant G.0431.10N. We thank M. Peumans and P. Pongprueksa for the translucency measurement, W. Veulemans for the flexural strength sample preparation, and J.W. Seo (MTM), S. Kuypers (JEOL) and Y. Ohnishi (JEOL) for the Al element STEM-EDS map (Fig .1b-3Y-0.25Al).

Reference

[1] Kelly JR. Ceramics in restorative and prosthetic dentistry. Annu Rev Mater Sci 1997;27:443-68.

[2] Zarone F, Russo S, Sorrentino R. From porcelain-fused-to-metal to zirconia: clinical and experimental considerations. Dent Mater 2011;27:83-96.

[3] Manicone PF, Rossi Iommetti P, Raffaelli L. An overview of zirconia ceramics: Basic properties and clinical applications. J Dent 2007;35:819-26.

[4] Miyazaki T, Nakamura T, Matsumura H, Ban S, Kobayashi T. Current status of zirconia restoration. Journal of Prosthodontic Research 2013;57:236-61.

[5] Zhang Y. Making yttria-stabilized tetragonal zirconia translucent. Dent Mater 2014;30:1195-203.

[6] Vichi A, Carrabba M, Paravina R, Ferrari M. Translucency of Ceramic Materials for CEREC CAD/CAM System. Journal of Esthetic and Restorative Dentistry 2014;26:224-31.

[7] Denry I, Kelly JR. State of the art of zirconia for dental applications. Dent Mater 2008;24:299-307.

[8] Studart AR, Filser F, Kocher P, Gauckler LJ. In vitro lifetime of dental ceramics under cyclic loading in water. Biomaterials 2007;28:2695-705.

[9] Piconi C, Maccauro G. Zirconia as a ceramic biomaterial. Biomaterials 1999;20:1-25.

[10] Garvie RC, Hannink RH, Pascoe RT. Ceramic steel. Nature 1975;258:703-4.

[11] Chevalier J, Cales B, Drouin JM. Low-Temperature Aging of Y-TZP Ceramics. J Am Ceram Soc 1999;82:2150-4.

[12] Chevalier J. What future for zirconia as a biomaterial? Biomaterials 2006;27:535-43.

[13] Lughi V, Sergo V. Low temperature degradation -aging- of zirconia: A critical review of the relevant aspects in dentistry. Dent Mater 2010;26:807-20.

[14] Al-Amleh B, Lyons K, Swain M. Clinical trials in zirconia: a systematic review. J Oral Rehabil 2010;37:641-52.

[15] Ross IM, Rainforth WM, McComb DW, Scott AJ, Brydson R. The role of trace additions of alumina to yttria–tetragonal zirconia polycrystals (Y–TZP). Scr Mater 2001;45:653-60.

[16] Fujisaki K, Kawamura K, Imai H. Zirconia powder for translucent dental zirconia: Zpex. Journal of Tosoh research 2012;56:57-61. DOI: http://www.tosoh.co.jp/technology/report/pdfs/2012_03_06.pdf (in Japanese).

[17] Baldissara P, Llukacej A, Ciocca L, Valandro FL, Scotti R. Translucency of zirconia copings made with different CAD/CAM systems. J Prosthet Dent 2010;104:6-12.

[18] Chen Y-M, Smales RJ, Yip KHK, Sung W-J. Translucency and biaxial flexural strength of four ceramic core materials. Dent Mater 2008;24:1506-11.

[19] Heintze SD, Rousson V. Survival of zirconia- and metal-supported fixed dental prostheses: a systematic review. Int J Prosthodont 2010;23:493-502.

[20] Guazzato M, Proos K, Quach L, Vincent Swain M. Strength, reliability and mode of fracture of bilayered porcelain/zirconia (Y-TZP) dental ceramics. Biomaterials 2004;25:5045-52.

[21] Beuer F, Stimmelmayr M, Gueth J-F, Edelhoff D, Naumann M. In vitro performance of full-contour zirconia single crowns. Dent Mater 2012;28:449-56.

[22] Zhang Y, Lee JJW, Srikanth R, Lawn BR. Edge chipping and flexural resistance of monolithic ceramics. Dent Mater 2013;29:1201-8.

[23] Preis V, Behr M, Hahnel S, Handel G, Rosentritt M. In vitro failure and fracture resistance of veneered and full-contour zirconia restorations. J Dent 2012;40:921-8.

[24] Samodurova A, Kocjan A, Swain MV, Kosmac T. The combined effect of alumina and silica co-doping on the ageing resistance of 3Y-TZP bioceramics. Acta Biomater 2014.

[25] Schechner G, Theelke B, Dittmann R, Herrmann A, Rolf J, Russell VA, et al. A New Class of Zirconia Material for Dental Application. J Dent Res : AADR annual meeting in Charlotte (Abstract #796) 2014.

[26] Communications A. Moving Target. Inside Dental Technology 2014;5.

[27] Klimke J, Trunec M, Krell A. Transparent Tetragonal Yttria-Stabilized Zirconia Ceramics: Influence of Scattering Caused by Birefringence. J Am Ceram Soc 2011;94:1850-8.

[28] Matsui K, Yoshida H, Ikuhara Y. Nanocrystalline, Ultra-Degradation-Resistant Zirconia: Its Grain Boundary Nanostructure and Nanochemistry. Sci Rep 2014;4.

[29] Nogiwa-Valdez AA, Rainforth WM, Zeng P, Ross IM. Deceleration of hydrothermal degradation of 3Y-TZP by alumina and lanthana co-doping. Acta Biomater 2013;9:6226-35.

[30] Guo X. Property Degradation of Tetragonal Zirconia Induced by Low-Temperature Defect Reaction with Water Molecules. Chem Mater 2004;16:3988-94.

[31] Matsui K. Grain-boundary structure and microstructure development mechanism in 2–8mol% yttria-stabilized zirconia polycrystals. Acta Mater 2008;56:1315-25.

[32] Hwang S-L, Chen IW. Grain Size Control of Tetragonal Zirconia Polycrystals Using the Space Charge Concept. J Am Ceram Soc 1990;73:3269-77.

[33] Anselmi-Tamburini U, Woolman JN, Munir ZA. Transparent Nanometric Cubic and Tetragonal Zirconia Obtained by High-Pressure Pulsed Electric Current Sintering. Adv Funct Mater 2007;17:3267-73.

[34] Eichler J, Rödel J, Eisele U, Hoffman M. Effect of Grain Size on Mechanical Properties of Submicrometer 3Y-TZP: Fracture Strength and Hydrothermal Degradation. J Am Ceram Soc 2007;90:2830-6.

[35] Shannon R. Revised effective ionic radii and systematic studies of interatomic distances in halides and chalcogenides. Acta Crystallographica Section A 1976;32:751-67.

[36] Garvie RC, Nicholson PS. Phase Analysis in Zirconia Systems. J Am Ceram Soc 1972;55:303-5.

[37] Toraya H, Yoshimura M, Somiya S. Calibration Curve for Quantitative Analysis of the Monoclinic-Tetragonal ZrO_2 System by X-Ray Diffraction. J Am Ceram Soc 1984;67:C-119-C-21.

[38] Kohorst P, Borchers L, Strempel J, Stiesch M, Hassel T, Bach F-W, et al. Low-temperature degradation of different zirconia ceramics for dental applications. Acta Biomater 2012;8:1213-20.

[39] Gremillard L, Chevalier J, Epicier T, Deville S, Fantozzi G. Modeling the aging kinetics of zirconia ceramics. J Eur Ceram Soc 2004;24:3483-9.

[40] Anstis GR, Chantikul P, Lawn BR, Marshall DB. A Critical Evaluation of Indentation Techniques for Measuring Fracture Toughness: I, Direct Crack Measurements. J Am Ceram Soc 1981;64:533-8.

[41] ISO standard 13356:2008. Implants for surgery -- Ceramic materials based on yttria-stabilized tetragonal zirconia (Y-TZP). ISO standard 13356 2008.

[42] ISO 6872:2008. Dentistry -- Ceramic materials. ISO 6872 2008.

[43] Della Bona A, Nogueira AD, Pecho OE. Optical properties of CAD-CAM ceramic systems. J Dent 2014;42:1202-9.

[44] Colorimetry: Understanding the CIE System. Canada: John Wiley & Sons, Inc., Hoboken, New Jersey; 2007.

[45] Guo X. Roles of Alumina in Zirconia for Functional Applications. J Am Ceram Soc 2003;86:1867-73.

[46] Boulc'h F, Djurado E, Dessemond L. Dopant Segregation and Space Charge Effect in Nanostructured Tetragonal Zirconia. J Electrochem Soc 2004;151:A1210-A5.

[47] Sakib Khan M, Saiful Islam M, R. Bates D. Cation doping and oxygen diffusion in zirconia: a combined atomistic simulation and molecular dynamics study. J Mater Chem 1998;8:2299-307.

[48] Zacate MO, Minervini L, Bradfield DJ, Grimes RW, Sickafus KE. Defect cluster formation in M_2O_3-doped cubic ZrO_2. Solid State Ionics 2000;128:243-54.

[49] Pezzotti G, Munisso MC, Porporati AA, Lessnau K. On the role of oxygen vacancies and lattice strain in the tetragonal to monoclinic transformation in alumina/zirconia composites and improved environmental stability. Biomaterials 2010;31:6901-8.

[50] Zimmermann A, Rödel J. Generalized Orowan-Petch Plot for Brittle Fracture. J Am Ceram Soc 1998;81:2527-32.

[51] Matsumoto M, Aoyama K, Matsubara H, Takayama K, Banno T, Kagiya Y, et al. Thermal conductivity and phase stability of plasma sprayed ZrO_2–Y_2O_3–La_2O_3 coatings. Surf Coat Technol 2005;194:31-5.

[52] Zhang F, Vanmeensel K, Inokoshi M, Batuk M, Hadermann J, Van Meerbeek B, et al. Critical influence of alumina content on the low temperature degradation of 2-3 mol% yttria-stabilized TZP for dental restorations. J Eur Ceram Soc 2014.

[53] Zhang H, Li Z, Kim B-N, Morita K, Yoshida H, Hiraga K, et al. Effect of Alumina Dopant on Transparency of Tetragonal Zirconia. Journal of Nanomaterials 2012;2012:5.

[54] Apetz R, van Bruggen MPB. Transparent Alumina: A Light-Scattering Model. J Am Ceram Soc 2003;86:480-6.

[55] Li P, Chen IW, Penner-Hahn JE. Effect of Dopants on Zirconia Stabilization—An X-ray Absorption Study: I, Trivalent Dopants. J Am Ceram Soc 1994;77:118-28.

Graphic abstract:

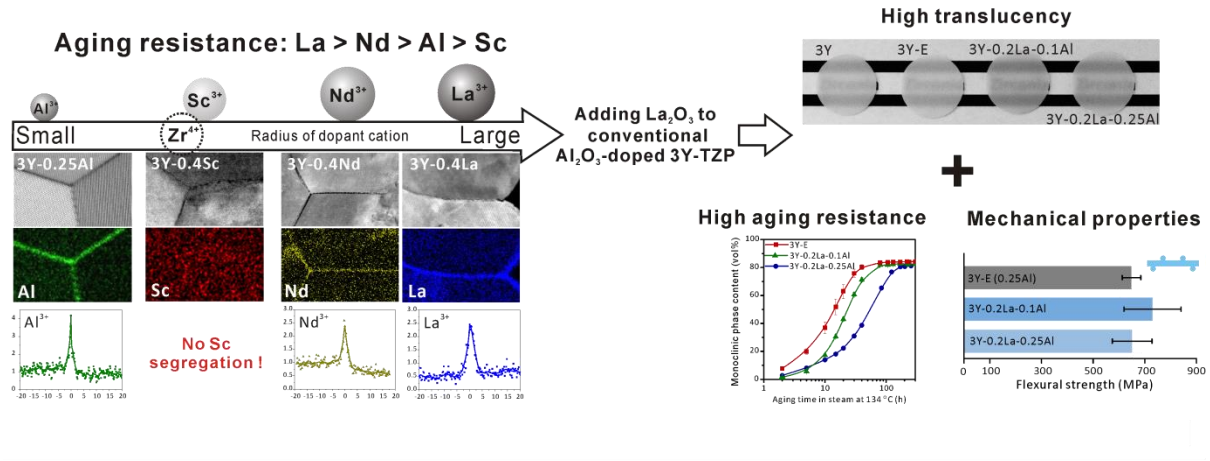

Figures:

Figure 1. Comparison of 3Y-TZPs doped with different trivalent oxides, sintered for 2 h at 1500 ℃: (a), Aging resistance, monoclinic phase content formed during accelerated aging at 134 ℃ as a function of the aging time. 0.2 mol% (left panel) or 0.4 mol% (right panel) Sc_2O_3, Nd_2O_3 and La_2O_3 were added to 3Y-TZP, and 0.25 wt% (0.3 mol%) Al_2O_3 was added for a direct comparison with commercial grade ceramics. Values of the ageing kinetic parameter b (h^{-1}) from JMA fitting are shown on the aging curves**. (b),** HAADF-STEM images, corresponding dopant STEM-EDS element maps, and elemental distribution profiles across the grain boundaries. **(c),** SEM images showing the grain size of the tetragonal zirconia doped with different trivalent dopants (scale bar 1 μm).

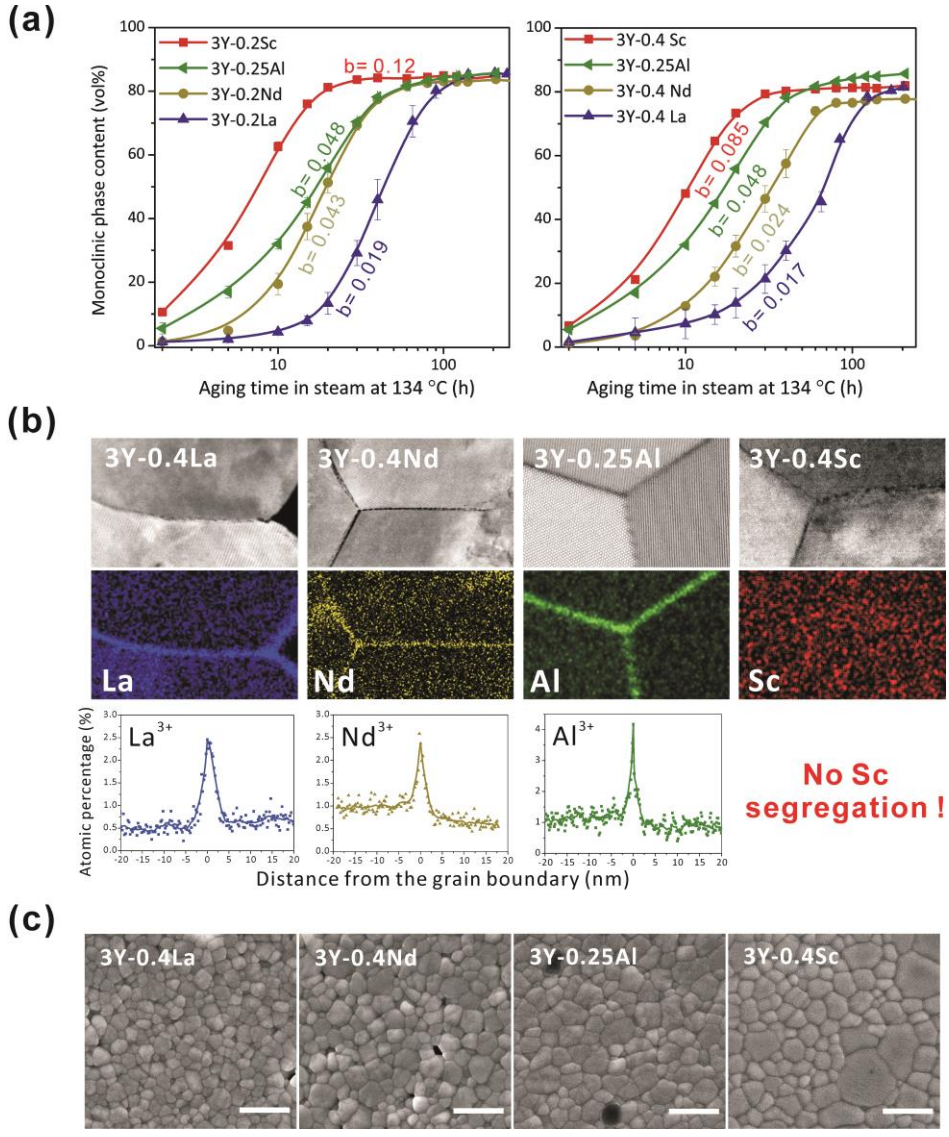

Figure 2. (a), Surface monoclinic phase transformation of 0.02-5 mol% La_2O_3-doped 3Y-TZPs sintered for 2 h at 1500 ℃ after 300 h accelerated aging at 134 ℃. The transformation rate decreased when the amount of La_2O_3 increased from 0.02 to 0.4 mol% (left) but increased when the amount of La_2O_3 was further increased (right). **(b),** Representative XRD patterns of non-aged 3Y-TZP doped with 0.02-5 mol% La_2O_3**.** A secondary $La_2Zr_2O_7$ phase was observed at > 1 mol % La_2O_3 doping.

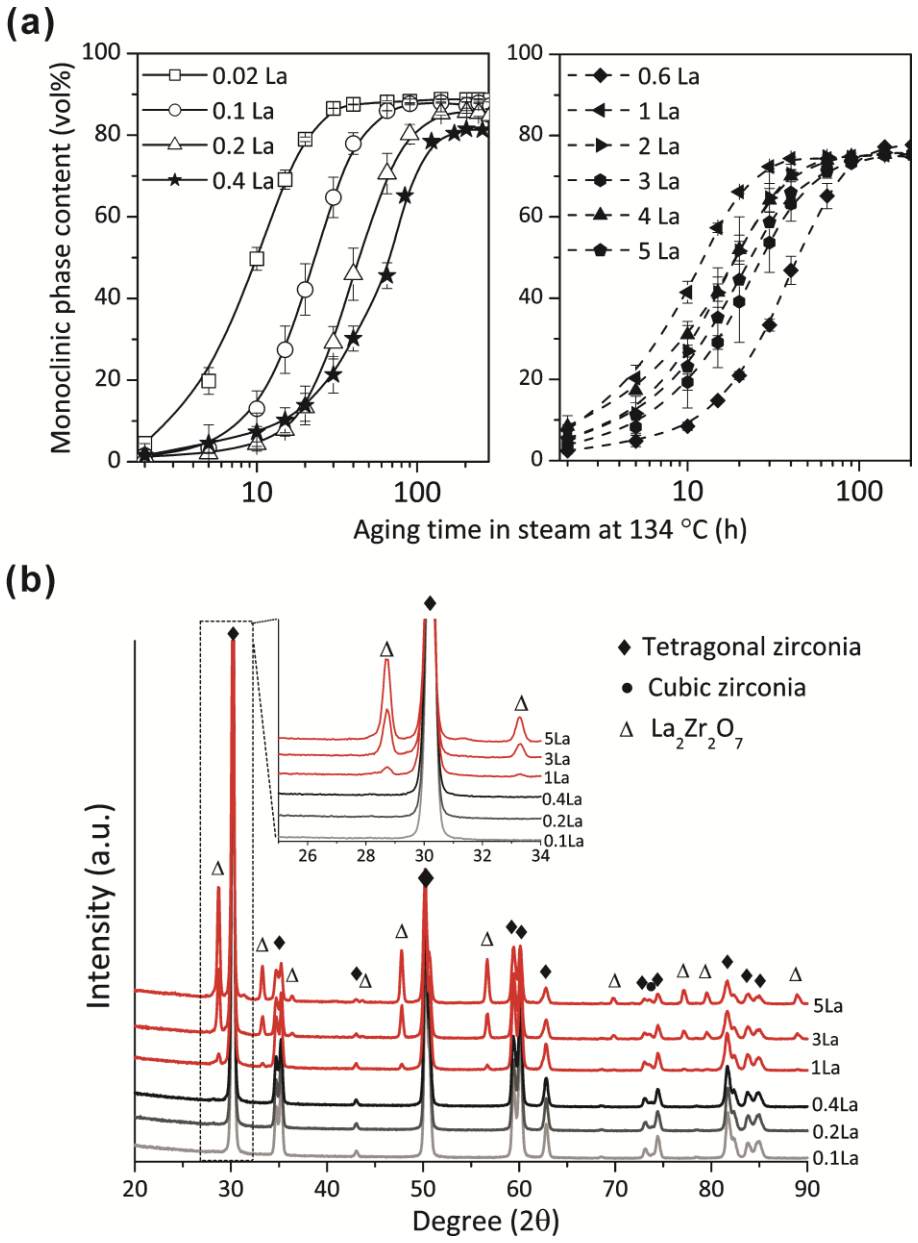

Figure 3. Comparison of 3Y-TZPs doped with La_2O_3 and Al_2O_3 and a reference 3Y-E (0.25Al) ceramic: (a), Aging resistance. The monoclinic phase content formed during accelerated aging at 134 ℃ are plotted as a function of the aging time for the ceramics sintered at 1450 and 1500 ℃; **(b),** Cross-sectional SEM images of La_2O_3 and Al_2O_3 co-doped 3Y-TZPs with ref. 3Y and 3Y-E (0.25Al) ceramics (sintered at 1450 ℃ without further surface treatment after the sintering process) after 500 h accelerated aging in steam at 134 ℃. The transformation depth in 3Y, 3Y-E, 3Y-0.2La-0.1Al and 3Y-0.2La-0.25Al was ≥43 μm, ~35 μm, <3 μm and <2 μm respectively. The photographs in the insets show that the surface of Ref. 3Y was delaminated; **(c),** Microstructures of the ceramics sintered at 1500 ℃, showing the sources of light scattering and the tetragonal zirconia grain size; (**d),** Translucency parameter of the ceramics sintered at 1500 ℃; **(e),** 4-point bending strength.

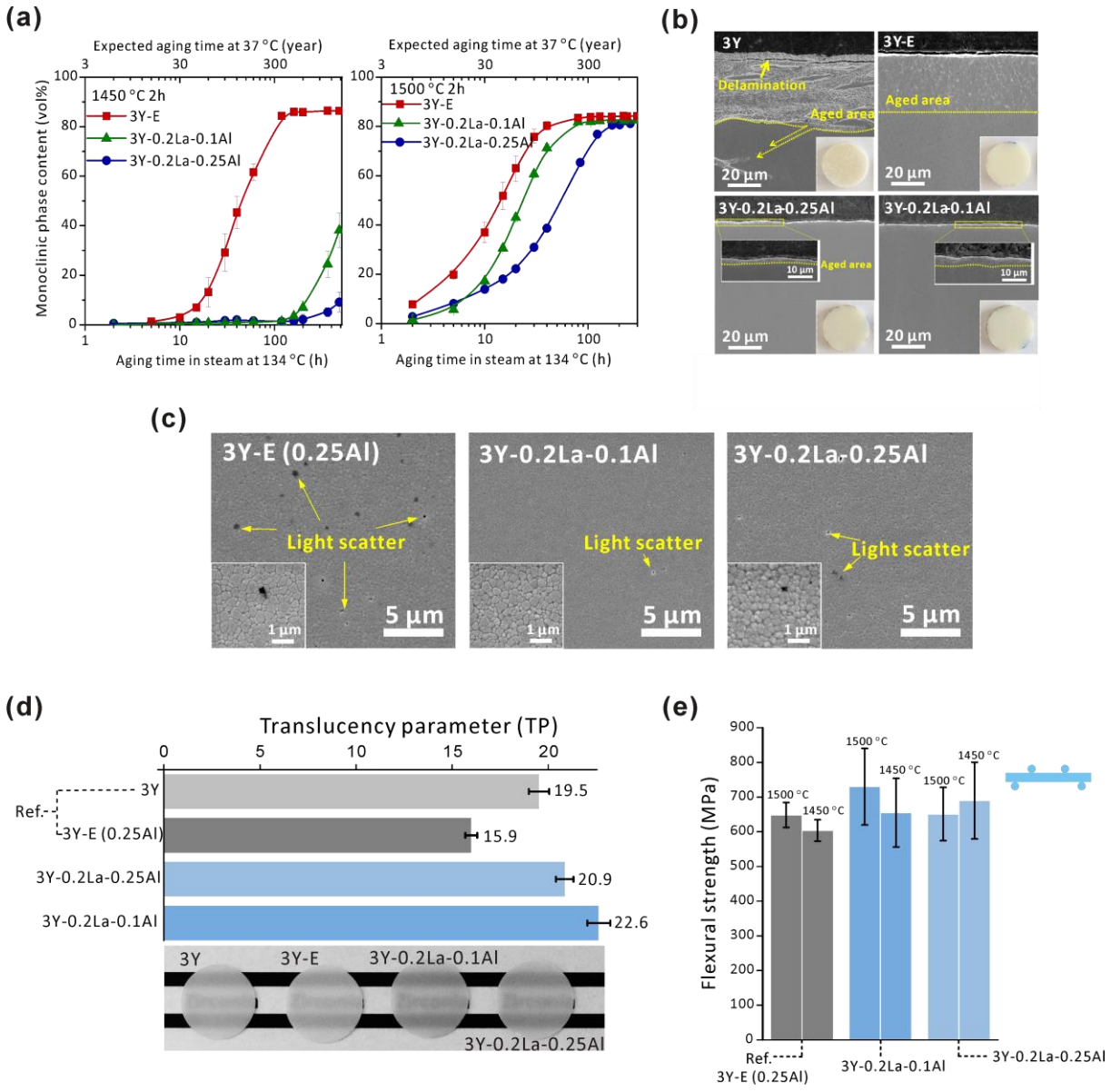

Tables

Table 1. Grain size, density, Vickers hardness, toughness and aging kinetic parameter b at 134 ℃ for La_2O_3-doped 3Y-TZPs with a La_2O_3 content from 0.02 to 5 mol%. V_{ms} is the monoclinic zirconia phase saturation level used in JMA fitting.

1500 ℃, 2h	Grain size (nm)	Density (g/cm^3)	Toughness ($MPa \cdot m^{1/2}$)	Hardness (kg/mm^2)	Aging kinetics	
					V_{ms} (%)	b (h^{-1})
3Y-0.02La	244 ±112	5.93 ±0.004	3.7 ±0.1	1156 ±31	88	0.082
3Y-0.1La	227 ±102	5.95 ±0.01	3.6 ±0.1	1203 ±27	87	0.038
3Y-0.2La	227 ±98	5.92 ±0.01	3.8 ±0.1	1178 ±30	85	0.019
3Y-0.4La	213 ±90	5.91 ±0.02	3.5 ±0.2	1128 ±39	81	0.017
3Y-0.6La	226 ±90	5.79 ±0.03	3.8 ±0.3	954 ±33	77	0.023
3Y-1La	232 ±103	5.77 ±0.02	3.6 ±0.1	1079 ±49	74	0.090
3Y-2La	224 ±98	5.71 ±0.02	4.0 ±0.4	932 ±43	74	0.057
3Y-3La	221 ±99	5.60 ±0.03	4.3 ±0.2	833 ±41	74	0.040
3Y-4La	252 ±135	5.52 ±0.04	3.6 ±0.2	847 ±32	74	0.061
3Y-5La	235 ±115	5.43 ±0.05	/	424 ±25	74	0.046

Table 2. Comparison of the ceramic translucency parameter (TP), contrast ratio (CR), roughness and thickness of 3Y-0.2La-0.1Al and 3Y-0.2La-0.25Al with Ref. 3Y and Ref. 3Y-E.

	3Y	3Y-E	3Y-0.2La-0.25Al	3Y-0.2La-0.1Al
Translucency parameter/TP	19.5 ±0.5	15.9 ±0.3	20.9 ±0.5	22.6 ±0.6
Contrast ratio /CR	0.54 ±0.01	0.61 ±0.01	0.48 ±0.01	0.52 ±0.01
Thickness (mm)	0.51 ±0.01	0.53 ±0.01	0.53 ±0.01	0.53 ±0.01
Roughness Ra (nm)	8 ±1	7 ±1	10 ±2	8 ±2

Table 3. Grain size, density and mechanical properties of La_2O_3 and Al_2O_3 co-doped 3Y-TZPs compared with the widely used Tosoh TZ-3Y-E based 3Y-TZP (3Y-E).

Ceramic	Sintering (℃)	Grain size of ZrO_2 (nm)	Density (g/cm^3)	Toughness ($MPa \cdot m^{1/2}$)	Hardness (kg/mm^2)	4-point bending strength (MPa)
3Y-E (0.25Al)	1500	305 ±127	6.04 ±0.01	3.4 ±0.1	1322 ±8	648 ±36
reference	1450	250 ±99	6.05 ±0.01	3.5 ±0.1	1331 ±11	604 ±31
3Y-0.2La-	1500	266 ±118	6.04 ±0.01	3.4 ±0.1	1304 ±17	651 ±77
0.25Al	1450	215 ±84	6.02 ±0.01	3.5 ±0.1	1331 ±14	690 ±111
3Y-0.2La-	1500	254 ±106	6.03 ±0.01	3.3 ±0.1	1347 ±13	730 ±111
0.1Al	1450	216 ±85	6.06 ±0.02	3.4 ±0.1	1358 ±16	655 ±99

"±" is standard deviation in all the tables.